Short-Term Performance of MM5 with Cloud-Cover Assimilation from Satellite Observations

ISMAIL YUCEL,* W. JAMES SHUTTLEWORTH, X. GAO, AND S. SOROOSHIAN

Department of Hydrology and Water Resources, The University of Arizona, Tucson, Arizona

(Manuscript received 1 May 2002, in final form 5 February 2003)

ABSTRACT

This study investigates the extent to which assimilating high-resolution remotely sensed cloud cover into the fifth-generation Pennsylvania State University–National Center for Atmospheric Research (PSU–NCAR) Mesoscale Model (MM5) provides an improved regional diagnosis of downward shortwave surface radiation fluxes and precipitation and enhances the model's ability to make short-range prediction. The high-resolution (4 km × 4 km) clear- and cloudy-sky radiances derived using a cloud-screening algorithm from visible band Geostationary Operational Environmental Satellite (GOES) data were used in the University of Maryland Global Energy and Water Cycle Experiment's Surface Radiation Budget (UMD GEWEX/SRB) model to infer the vertically integrated cloud mass via cloud optical thickness. Three-dimensional cloud fields were created that took their horizontal distribution from the satellite image but derived their vertical distribution, in part, from the fields simulated by MM5 during the time step immediately prior to assimilation and, in part, from the observed cloud-top height derived from the infrared band of GOES. Linear interpolation was used to derive 1-min cloud images between 15-min GOES samples, and the resulting images were ingested every minute. Comparisons were made between modeled and observed data taken from the Arizona Meteorological Network (AZMET) in southern Arizona for model runs with and without cloud ingestion. Cloud ingestion substantially improved the ability of the MM5 model to capture temporal and spatial variations in surface fields associated with cloud cover. Experiments in which the model was operated in forecast mode suggest that cloud ingestion gave some limited enhancement in MM5 short-term prediction ability for up to 3 h. However, an analysis suggests that, in order to get additional forecasting capability, it will be necessary to modify the atmospheric dynamics and thermodynamics in the model to be consistent with the ingested cloud fields.

1. Introduction

Mesoscale meteorological models have been used extensively to study cloud and convective precipitation for a range of geographical conditions over continents. Although sophisticated cloud-resolving techniques can be used to parameterize cloud and precipitation, the largest source of uncertainty in mesoscale clouds remains in predicting convective systems at high spatial resolution. This uncertainty is particularly severe when models are applied in the semiarid regions of the southwestern United States during the summer monsoon because of the strong insolation and the presence of elevated heat sources associated with the complex topography. In this region, convection often forms over high terrain (Watson et al. 1994) and is then modified by the ambient flow, complex orography, and the local environment (Smith and Gall 1989). Clouds, and their effect on the surface energy budget in mesoscale meteorological models, are the topic of discussion and research in several studies (e.g., Lipton 1993; Lipton and Modica 1999; Ruggiero et al. 2000). These studies reveal that surface energy exchanges, which depend on overlying cloud cover, have a strong impact on the mesoscale processes that most affect the short-term prediction of clouds and precipitation.

On the other hand, it is now recognized that incorporating satellite data into the numerical weather forecast models can yield improved documentation of mesoscale cloud radiative properties and precipitating systems. In due course, such improved skill may provide the basis for the real-time application of a hydrometeorological system capable of predicting flash floods, these being a significant threat to life and property during the monsoon period in the southwestern United States. In this context, Yucel et al. (2002) investigated the influence of clouds on the surface energy and water balance through time-continuous assimilation of cloud cover retrieved from the visible band of Geostationary Operational Environmental Satellite (GOES). They demonstrated that this had beneficial effects on the anal-

* Current affiliation: Center for Atmospheric Sciences, Hampton University, Hampton, Virginia.

Corresponding author address: Ismail Yucel, Center for Atmospheric Sciences, Hampton University, Hampton, VA 23668.
E-mail: ismail.yucel@hamptonu.edu

TABLE 1. The primary relevant features of MM5 as applied in this study.

Category	Options used	References
Stable precipitation	Explicit microphysics	Tao–Simpson (1993)
Convective parameterization	None (4 km)	
	Kain–Fritsch (12 km)	Kain and Fritsch (1992)
Radiation	Dudhia	Dudhia (1989)
Surface layer	OSU/ETA	Chen and Dudhia (2001)
Boundary layer	MRF	Hong and Pan (1996)

ysis given by the Regional Atmospheric Modeling System (RAMS). That study did not deal with the forecast issue explicitly, but assimilation ensured that the impact of clouds on the surface energy and water balance was appropriately represented during the analysis and, to some extent, prior cloud ingestion resulted in enhanced short-term model forecasts of cloud cover.

The goals of the research reported here were to extend cloud-cover assimilation to a new model and, by making comparison with field data, to study the effect on the quality of diagnosed fields and to investigate the impact of prior cloud-cover ingestion on short-term forecasts of cloud and precipitation. Vertically integrated cloud water/ice fields derived (via optical depth) from the visible band of GOES using the University of Maryland (UMD) Global Energy and Water Cycle Experiment's Surface Radiation Budget (GEWEX/SRB) model were ingested directly into the, fifth-generation Pennsylvania State University–National Center for Atmospheric Research (PSU–NCAR) Mesoscale Model (MM5). Clouds are distributed in the vertical starting from the cloud top, which is derived from the infrared band of GOES. The impact on the model's ability to diagnose surface radiation and precipitation fields was investigated through comparisons between observed and modeled data, with and without cloud ingestion, for the period 14–15 July 1999, when there were significant changes in cloud cover. Finally, a test was made of the improvement in short-term predictions of cloud cover and precipitation given by ingesting cloud data into MM5 prior to predictive runs.

2. Description of model and study area

a. Mesoscale atmosphere model

Version 3.4 of MM5 (Dudhia 1993; Grell et al. 1995) was used in this study. The model is nonhydrostatic, with a terrain-following $\sigma - p$ coordinate system, and includes a two-way interactive, movable nested grid (Smolarkiewicz and Grell 1992). Development and verification of MM5 have been carried out in many applications, including Liu et al. (1997) and Colle et al. (1999, 2000), which are recent studies focused on the prediction of precipitation and cloud microphysics at high spatial resolution.

The MM5 was employed in a two-way interacting nested configuration with 60×60 grid points at 12-km and 100×100 grid points at 4-km resolutions, with its fine-sized domain covering the semiarid region of interest in southern Arizona. The model was initiated, and time-varying lateral boundaries for the coarse domain then nudged every 6 h, using 40-km analysis fields from the National Centers for Environmental Prediction's (NCEP's) Eta Model. A high-resolution (<0.5 km grid) dataset was used to characterize modeled land surface across the fine-grid domain, while the modeled atmosphere was described at 23 σ levels, these being distributed more frequently in the lower levels to ensure that resolution in the boundary layer is adequate for use of the planetary boundary layer (PBL) scheme. The primary, relevant features of MM5 as applied during this study are given in Table 1.

Cloud and precipitation processes were parameterized using the Tao–Simpson (1993) microphysical scheme, with the Kain–Fritsch (1992) cumulus parameterization used on the 12-km domain. The Tao–Simpson (1993) microphysics scheme, which is modified from Lin et al. (1983), contains prognostic equations for air temperature and hydrometeor classes (i.e., cloud water, rainwater, pristine ice, snow, and graupel within clouds). The thermodynamic energy equation is based on Orville and Kopp (1977) and includes terms representing the advection, turbulent mixing, heating effect due to phase change, and energy changes due to the various hydrometeors coming into thermal equilibrium with the environment. The scheme allows for the generation of supercooled water. Cloud water and pristine ice are nonprecipitating fields because their terminal velocities are assumed to be small when compared with that of rain, snow, and graupel that have appreciable terminal velocities. The mixing ratios of each cloud hydrometeor class are predicted by applying time-dependent mass continuity equations, which include advective, diffusive, and production terms. The last term is the source and sink, and describes the rates of conversion of water between phases and hydrometeor types.

In this study, radiative fluxes were calculated using a single broadband radiation model developed by Dudhia (1989). This scheme is based on the computation of infrared emission and visible reflection that both interact with the atmosphere, including the cloud and precipitation fields, as well as with the surface. While water vapor is the primary absorber in clear air, in cloudy atmospheres, absorption and scattering by cloud hydrometeors is substantial and modulates the atmospheric radiational cooling and heating profiles.

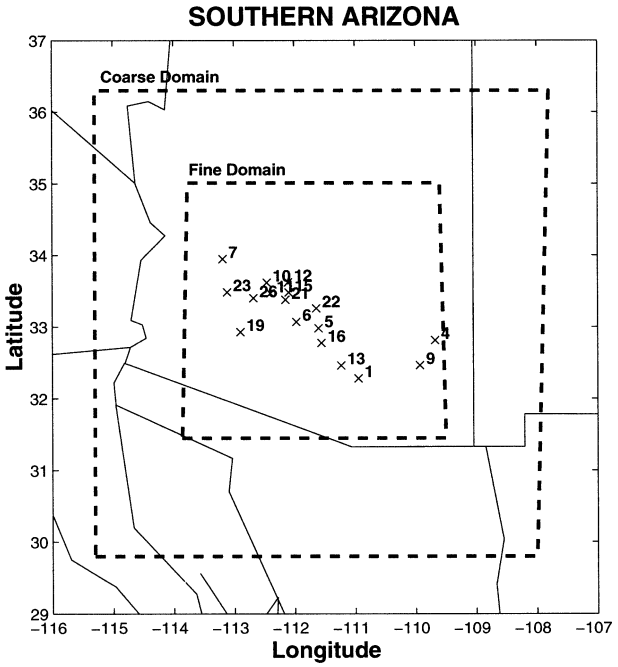

FIG. 1. The study area modeled in the nested configuration of MM5 and the location of the AZMET field sites.

b. Study area

The study area comprised the region between 31.5° and 36°N and 108° and 115°W in southern Arizona. The semiarid environment at this study site is due both to its location relative to the equator and the orographic drying effect of mountain ranges in the western United States. The region is characterized by rugged mountain ranges separated by flat valley floors. The limited annual rainfall of less than 400 mm occurs mainly as convective thunderstorms in a summer monsoon season and as frontal storms during the winter.

Observations are taken from the Arizona Meteorological Network (AZMET) system. These measurement stations are often installed adjacent to regions of irrigated agriculture, and the data may, in part, be influenced by this fact. In this study, data from 17 individual stations were used, concentrated near the center of the study area (Fig. 1). Information on the location, elevation, and soil composition of these sites is provided in Table 2. The data used in this study were hourly measurements of downward surface solar radiation and precipitation. Solar radiation is measured using Licor LI200S Pyronometers, while precipitation is recorded using RG2501 tipping-bucket rain gauges. (More detailed information on the AZMET observational network is available online at http://ag.arizona.edu/azmet/.)

A sample of vertical reflectivity values measured by a Doppler radar system located in the study area, at coordinates 110.63°W and 31.89°N, was compared with model-predicted cloud profiles. The radar system, with wavelength 10 cm and sampling frequency 5 min, is deployed at an elevation of 1616 m on a mountain near Tucson, Arizona. The sample data used in this study were collected with the system operating with elevation angles between 0.48° and 19.51°, azimuth angles between 280° and 310°, with a beam width of 1°, and with ranges (distance from radar) every 1 km between 10 and 90 km. Thus, the reflectivity data are available at different levels for each azimuth angle at 1-km intervals along the 90-km path, and reflectivity profiles were averaged and interpolated, as appropriate, to match the modeled cloud fields at 4-km resolution.

3. Satellite-based cloud retrievals

The reflected visible (0.55–0.75 μm) radiances available every 15 min at 1-km resolution from *GOES-10* were used to retrieve high-resolution (4 km × 4 km)

TABLE 2. Location and elevation of the observation sites in the southern Arizona (AZMET) area used in this study.

Station (#)	Coordinates lat, lon	Elevation (m)	Soil particle size: Sand (%)	Silt (%)	Clay (%)	Soil texture type
Tucson (01)	32.28°N, 110.946°W	713	64	26	10	Sandy loam
Queen Creek (22)	33.258°N, 111.642°W	430	—	—	—	Analysis not complete
Harquahala (23)	33.483°N, 113.116°W	350	—	—	—	Analysis not complete
Safford (04)	32.813°N, 109.69°W	901	46	30	24	Loam
Coolidge (05)	32.98°N, 111.605°W	422	62	25	13	Sandy loam
Maricopa (06)	33.069°N, 111.972°W	361	—	—	—	Analysis not complete
Aguila (07)	33.947°N, 113.189°W	655	31	34	35	Clay loam
Buckeye (26)	33.40°N, 112.68°W	304	—	—	—	Analysis not complete
Bonita (09)	32.4636°N, 109.929°W	1346	77	16	7	Loamy sand
Waddell (10)	33.618°N, 112.460°W	407	60	30	10	Sandy loam clay
Litchfield (11)	33.467°N, 112.398°W	309	66	23	11	Sandy clay loam
Pheonix Greenway (12)	33.621°N, 112.108°W	401	—	—	—	Analysis not complete
Marana (13)	32.461°N, 111.233°W	601	—	—	—	Silt clay loam
Phoenix Encanto (15)	33.479°N, 112.096°W	335	—	—	—	Analysis not complete
Eloy (16)	32.774°N, 111.557°W	461	—	—	—	Analysis not complete
Paloma (19)	32.927°N, 112.896°W	219	—	—	—	Analysis not complete
Laveen (21)	33.376°N, 112.15°W	315	—	—	—	Analysis not complete

fields of cloud cover and associated cloudy- and clear-sky radiance maps using an automated cloud-screening algorithm. The procedure used a real-time tracking technique to determine the required clear-sky composite images and involved threshold statements to discriminate radiance samples into cloudy, clear, and mixed categories. The high-resolution, derived fields of cloudy- and clear-sky radiances and cloud fraction were used in the UMD GEWEX/SRB model (Whitlock et al. 1995; Pinker and Laszlo 1992) to infer the vertically integrated optical depth. Optical depths are determined by matching the broadband top-of-the-atmosphere albedo under clear and cloudy skies, with the computed albedo available in lookup tables. The model uses predefined cloud optical thickness values (ranging from 0 to 500), which were originally derived by Stephens (1978) for a set of eight different ''standard'' cloud types. Stephens (1978) then derived an empirical equation between cloud mass and the broadband optical thickness of these cloud types for the two spectral regions (0.3–0.7 and 0.75–4 μm). In this study, vertically integrated cloud water and ice fields were calculated using the relationship for the first spectral region where conservative scattering is dominant. For a more detailed description of satellite-derived cloud retrievals, the reader is referred to Yucel et al. (2002). In addition to the visible band, the emitted infrared (10.20–11.20 μm) radiance measured by *GOES-10* with a spatial resolution of 4 km was used to determine cloud-top brightness temperature.

4. Updating cloud microphysics in MM5

A variety of data assimilation techniques have been used to initiate numerical weather prediction (NWP) models prior to short-range (0–12 h) weather forecasts. To allow clearer appreciation of the role and value of using remotely sensed cloud-cover data in this study, we opted to use the nudging assimilation technique in preference to the more complex variational data assimilation technique. The assimilation method is an extension of that used by Yucel et al. (2002), but it differs in that, in addition to the visible band, it uses the infrared band of GOES to determine cloud-top brightness temperature and height. It was shown by Albers et al. (1996) in the Local Analysis and Prediction System (LAPS) that combining the number of observed data sources and assimilating them into numerical weather prediction models improve these model's simulations further. The method developed in this study, for example, provides a three-dimensional depiction of the water content in several phases of cloud (liquid, rain, ice, snow, and graupel) based on both modeled fields and the GOES retrievals. Using the GOES infrared band brightness temperature allowed clouds (which can be warm, cold, or mixed) to be distributed relative to the observed cloud-top heights. Cloud assimilation was only carried out in the 4-km-resolution inner model domain, but its feedback is provided to the coarse domain via the model. Cloud fields were linearly interpolated between 15 min GOES images and ingested into the MM5 every minute because high-frequency assimilation was shown to give noticeably better results in our previous study (Yucel et al. 2002). The MM5 simulation started on 13 July 1999 at 1700 local time and ended on 15 July 1999 at 1700 local time, with cloud ingestion during the daylight hours between 7000 and 1645 local time.

a. Deriving cloud-top and cloud-base heights

Infrared satellite data were used to retrieve the altitudes of the cloud tops. Derivation of cloud-top altitude depends on the relationship between the cloud's altitude and its temperature. This relationship was specified on an area-average basis across the modeled domain, assuming that MM5 calculates the vertical profile of air temperature correctly in the time step immediately prior to cloud assimilation. The cloud-top brightness temperature for each cloud-covered grid square (derived from satellite infrared radiance) is then used to identify cloud-top layers in the modeled atmosphere.

The distance between cloud top and cloud base was estimated assuming that there is only one cloud layer and that the vertical distribution of the cloud water/ice, whose magnitude is derived from visible imagery, is that which would be produced by moist-adiabatic ascent from cloud base to cloud top. Thus, it was assumed that air in the first MM5 level below the cloud top is saturated at the temperature and pressure of that level. The total condensed cloud water, W_m, is computed by moist-adiabatic ascent between that level and the cloud-top level, and this is compared with W_s, the total cloud water/ice estimated from the satellite observation for this grid square. If $0.3W_m < W_s$, [Note: 0.3 is a constant whose value varies between 0.1 and 1.0 in the literature; see Lipton and Modica (1999) and Frisch et al. (1995)], then the next level down is also assumed saturated and W_m is recomputed. This process is repeated until the inequality is reversed (i.e., $0.3W_m > W_s$). The level at which this reversal occurs is then the cloud base for the grid square. The value of W_m is the theoretical maximum of total condensed cloud water for an ascent through a specified layer. The lower the value of the constant in the inequality used when calculating cloud depth, the lower the computed cloud-base height. In this study, the condensed cloud water is assumed to be 30% of the theoretical maximum because the computation is for deep summertime convective clouds. In practice, the cloud-base height calculated assuming the value 0.3 was always above the ground in the modeled atmosphere.

b. Updating model cloud microphysics from satellite observations

Details of the methods used to update model cloud microphysics are given in the appendix; here, we provide only an overview of the strategy used. Because

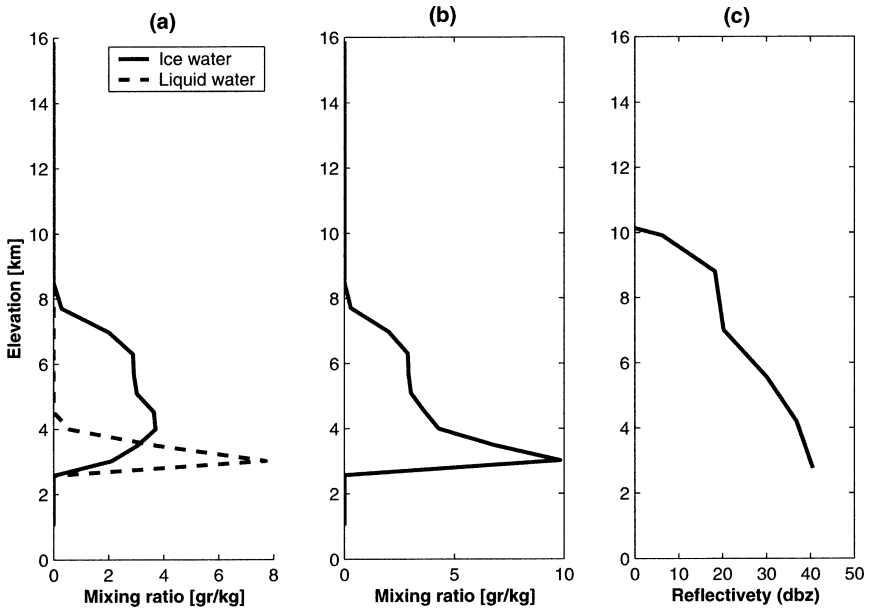

FIG. 2. At a selected model grid, the vertical profiles of MM5 cloud microphysics calculated in the cloud-assimilation algorithm (a) for frozen (pristine ice, snow, graupel) and liquid water (cloud, rain), and (b) for total cloud water (cloud water, rain, pristine ice, snow, graupel). (c) The radar reflectivity profile at the same grid point.

satellite images only provide information on the horizontal position of cloud fields in the model domain, it is necessary to define an algorithm for distributing the cloud water/ice vertically in each modeled grid square between the cloud top and cloud bottom, determined as described in the previous section. The cloud water/ice fields were distributed from cloud top to base heights as warm (cloud water, rainwater), cold (pristine ice), or mixed (cloud, rain, pristine ice, snow, graupel) hydrometeors, based on the brightness temperatures obtained from the GOES infrared image. High-level, cold clouds, whose cloud-top height may be similar to convective clouds, are diagnosed from satellite-derived cloud optical depth and brightness temperature. They are assumed present if the cloud top is above the freezing level and the optical depth is less than 10 (a typical optical depth for cirrus clouds). The following four different methods were used to update the cloud microphysics in MM5 in this study.

1) In the case of a 4 km $\times$ 4 km grid square in which both the satellite image and MM5 indicate no cloud is present, no change was made to MM5 variables for the grid square.
2) In the case of a 4 km $\times$ 4 km grid square in which the satellite image indicates cloud and MM5 also simulates cloud along the specified cloud layer, it was assumed that MM5 calculates the relative proportions of different cloud species correctly, even though it miscalculates the total amount of cloud water/ice. Thus, the procedure was to increase or decrease the modeled mass of each species of cloud water/ice simulated in MM5 at all levels in the cloud column until the mass of cloud water/ice simulated in the model was equal to that estimated from the satellite.
3) In the case of a 4 km $\times$ 4 km grid square in which the satellite image indicates there is no cloud but MM5 simulates cloud, the cloud water/ice in MM5 was set to zero for all cloud water species at all levels in the grid square.
4) In the case of a 4 km $\times$ 4 km grid square in which the satellite image indicates cloud but MM5 does not simulate cloud, the method used to calculate cloud-base altitude was adopted. Thus, the amount of condensed water computed for moist adiabatic ascent from the cloud base to the cloud top was matched to the satellite-derived cloud water/ice and all assigned to the liquid water species in MM5, with other cloud water species set to zero. In practice, MM5 quickly reassigns the liquid water between different cloud water species and model levels.

With cloud-cover ingestion, MM5 responds rapidly to the assimilated image and locates cloud where it is observed to be; hence, the less dramatic of the previous procedures, that is, procedures 1) and 2), rapidly become those most commonly used.

As a test of the procedures used for distributing cloud vertically in MM5, the vertical profiles of cloud simulated by MM5 after cloud ingestion were compared to the radar reflectivity profile for a selected 4-km model grid square at 1800 UTC 15 July 1999. The results are shown in Fig. 2. Because both ice (pristine ice, snow,

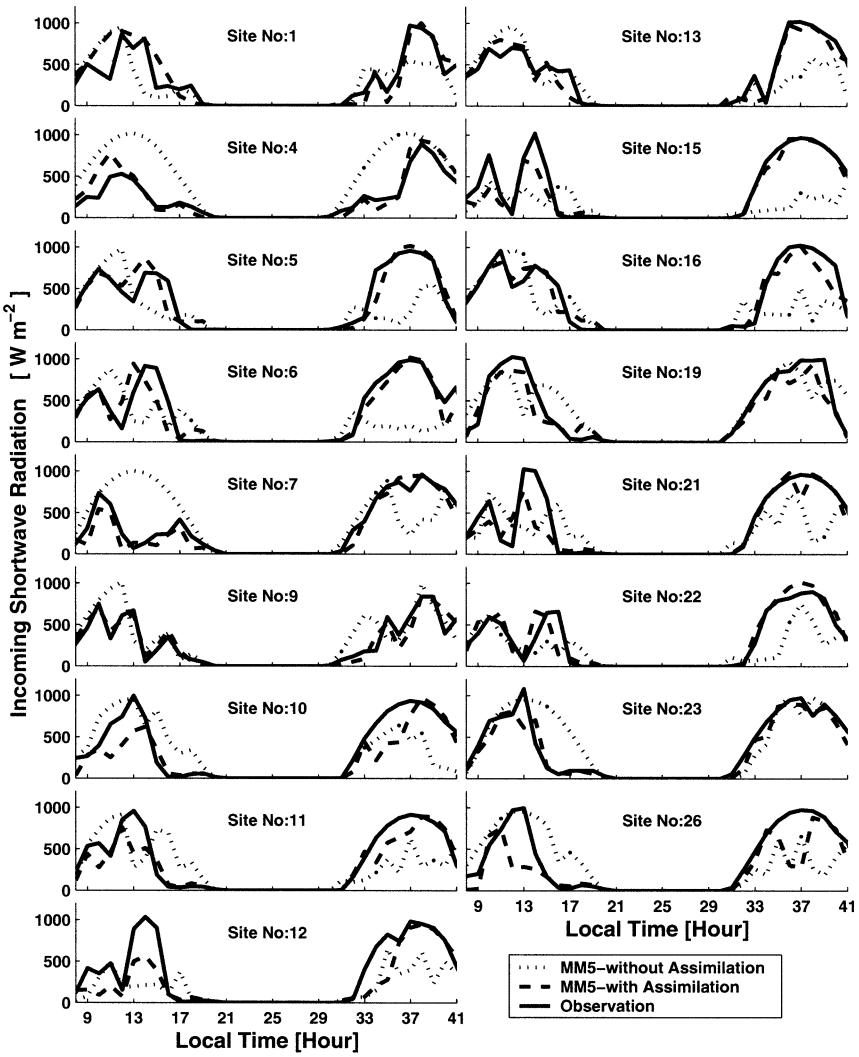

FIG. 3. Incoming surface solar radiation observed at the AZMET sites compared with the equivalent modeled values, with and without cloud-cover assimilation, during the period 14–15 Jul 1999.

graupel) and liquid (cloud water, rain) components of clouds were simulated by MM5 in this grid square immediately prior to cloud ingestion, ingestion method (b) mentioned earlier was being used in this case. The vertical cloud profile (Figs. 2a,b), with a minor maximum at high altitude and major maximum at lower altitudes, that is obtained when the modeled cloud fields are revised by satellite observations, is broadly similar to the radar reflectivity profile (Fig. 2c). A melting layer height of 4.5 km is suggested by the radar reflectivity profile, because the size of hydrometeor particles is enlarged by raindrops and the radar echo increases quickly. Typically radar reflectivity is enhanced in a melting layer due to the phase change of the hydrometeors from frozen to liquid even if the total water content remains constant. Similar behavior is seen in the modeled cloud fields, with ice hydrometeors, graupel, and snow falling from higher levels into a melting layer where the concentration of rainwater increases rapidly. Based on the brightness temperature of 247.7 K, for this model grid, the derived cloud-top height is 10.2 km (sigma layer 20) and the optical thickness is 500, indicating that the ingested cloud is likely of convective origin. It is also important that, because the reflectivity is from a composite of successive scans at different elevations, the profile is resolved more coarsely than it would be with a vertically pointing radar.

5. Results

a. Impact of cloud assimilation on energy and water balance in the fine domain surface

1) INCOMING SHORTWAVE RADIATION

Figure 3 shows the hourly average surface shortwave radiation modeled by MM5 on 14–15 July 1999, with

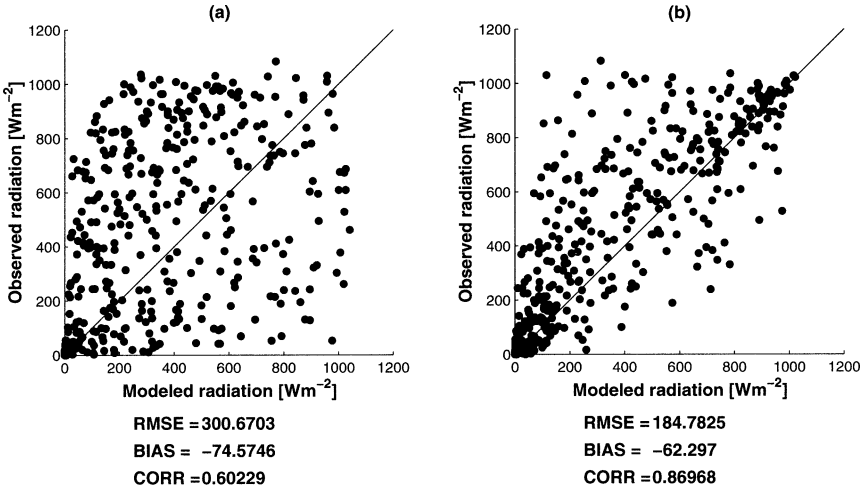

FIG. 4. Comparison between modeled and observed hourly average daytime surface solar radiation for model simulations (a) without cloud assimilation and (b) with cloud assimilation corresponds to the period 14–15 Jul 1999. In each case, the correlation coefficient, root-mean-square error, and mean bias are given.

and without cloud ingestion, compared with values observed at AZMET sites. It is apparent that the model did not correctly capture the diurnal variation of surface solar radiation at AZMET sites when there was no assimilation of satellite observations because the modeled overlying cloud cover was wrongly located in the model domain. However, this was substantially improved by cloud ingestion because cloud cover in the model grid square was better represented. Thick convective clouds, simulated during the control run over sites 1, 5, 6, 13, 15, 16, 21, and 22 on 15 July are, for example, removed and replaced with nonprecipitating clouds with cloud ingestion. In this case, the observed cloud brightness temperature ($T_{b_{i,j}}$) is less than 250 K and cloud optical thickness ($\tau_{i,j}$) is less than 10, assumed in the cloud ingestion scheme. The improvement obtained by cloud ingestion is also apparent in Fig. 4, which shows the hourly average modeled and observed surface solar radiation at all sites. On average, over the period for which comparison was made, ingesting remotely sensed cloud cover improves the root-mean-square error (rmse) between modeled and observed values from 300.67 to 184.78 W m^{-2}, the bias from -74.57 to -62.29 W m^{-2}, and the correlation coefficient from 0.60 to 0.87.

2) PRECIPITATION

Figure 5 shows a comparison between the precipitation observed at the AZMET sites and that calculated by MM5 with and without cloud assimilation, for 14–15 July 1999. Without cloud-cover ingestion, MM5 consistently underestimated surface precipitation at the AZMET sites. However, the timing and, to some extent, magnitude of the modeled precipitation were captured better when satellite visible and infrared observations of cloud were ingested. The storms simulated by MM5 were then approximately in the right place and right time. Because the model diverges from reality without frequent assimilation of information, the nighttime storms (~20 mm) observed at sites 7 and 11 were not captured by MM5.

Ice particles play an important role in the formation of precipitation and, with cloud assimilation, MM5 produced more rainfall than observed at sites 1, 4, 9, and 10 because graupel, the cloud ice hydrometeor in mixed clouds where ingestion procedure recognizes $T_{b_{i,j}}$ is less than 273 K, and $\tau_{i,j}$ is greater than 10, falls rapidly into the melting layer, which enhances surface precipitation. On the other hand, the peak values at sites 1, 6, 15, and 21 were not captured with cloud assimilation because some of the rainwater is lost by evaporation at the lower model levels at semiarid sites. Clearly, model-calculated surface precipitation is therefore very sensitive to the vertical position of cloud and to interaction between the hydrometeors, and poor representation of these within-cloud features cannot be corrected merely by ingesting cloud-cover data alone.

Precipitation observations are point measurements and, to minimize the consequences of this in the comparison, Fig. 6 shows the site-average modeled and observed precipitation for 14–15 July 1999. When averaged over all sites, the timing and magnitude of rainfall are at least broadly correct with cloud-cover ingestion.

b. Impact of prior cloud assimilation on short-term forecasts

1) CALCULATING FORECAST CLOUD-COVER FIELDS

The impact of ingesting satellite-derived cloud cover every minute for 3 h on short-range predictions of cloud cover and precipitation was investigated. In fact, frac-

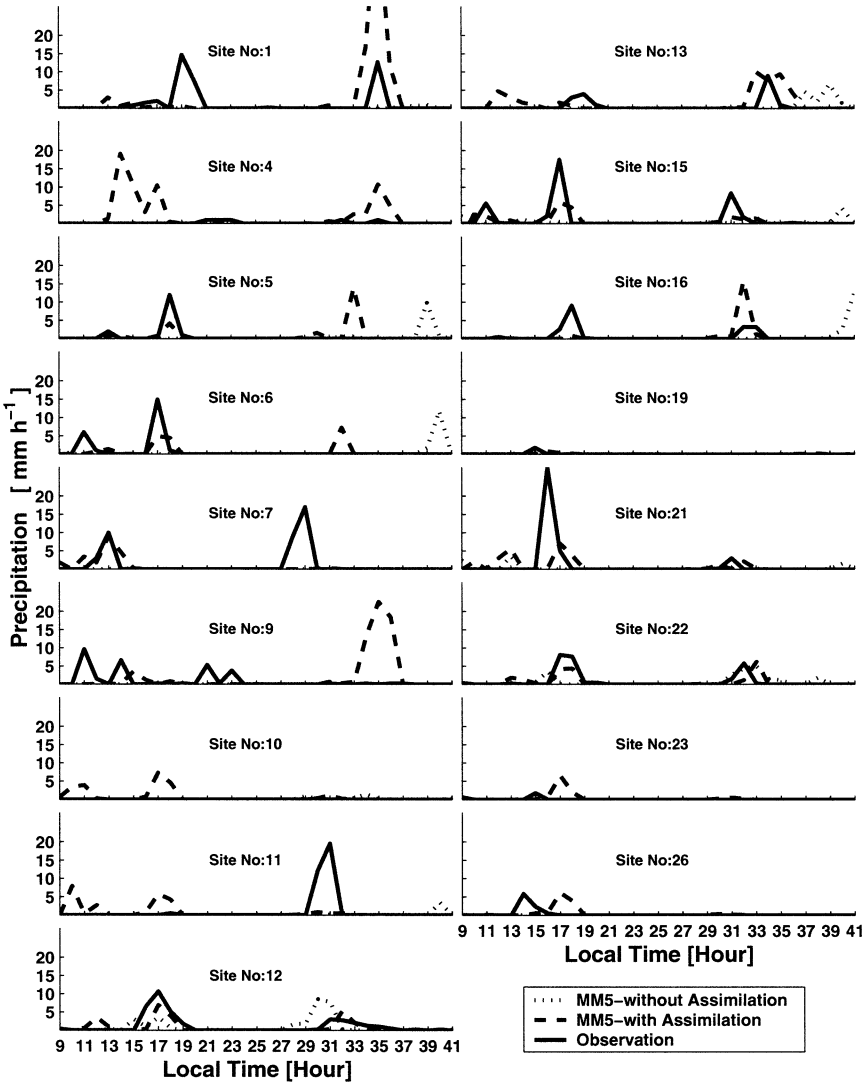

FIG. 5. Precipitation observed at the AZMET sites compared with the equivalent modeled values with and without cloud-cover assimilation during the period 14–15 Jul 1999.

tional cloud-cover fields are not available in MM5. Consequently, for the purpose of this test, they were derived for each 4 km × 4 km grid using a time- and location-specific relationship between satellite-retrieved total cloud mass and fractional cloud cover calculated for the period of the study. The forecast values of the mixing ratios for different types of cloud microphysics in all the atmospheric columns in the modeled domain were converted to the vertically integrated mass fields, and then the corresponding fractional cloud cover was calculated in this time- and location-specific relationship. A skill score was defined based on the match between modeled and observed fractional cloud cover across the model domain, the level of success being specified by the equation

$$\text{Success} = \frac{1}{N}\sum_{i=1}^{N}(100 - 100|f_i^m - f_i^s|),$$

where f_i^m and f_i^s are modeled and satellite-derived fractional cloud cover, respectively. This skill assessment was applied for the grid squares that were observed to be cloudy.

2) EVALUATION OF CLOUD COVER AND PRECIPITATION FORECAST

Figure 7 shows a comparison between the forecast fractional cloud cover with and without prior cloud-cover ingestion from satellite observations, together with the observed cloud fraction derived from the GOES satellite images every 15 min for a 4.5-h forecast period. Figure 8a shows the skill scores for these comparisons. As the density of the observed clouds spreads to cover much of the modeled domain as the forecast time increases, the skill scores from the MM5 forecast reduce. The model forecast with prior ingestion of satellite data

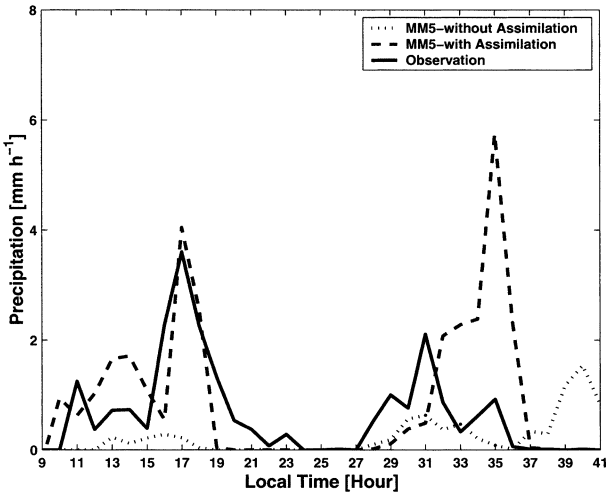

FIG. 6. Site-average modeled and observed precipitation are compared for 14–15 Jul 1999.

shows a small but significant improvement in skill when forecasting clouds in the early hours of the forecast period relative to the standard MM5 forecast. However, the skill score for the run with prior cloud-cover ingestion drops sharply from 100% to 74% during the first 15 min of the forecast, and then remains 5% to 10% better than the standard forecast for about the next 4 h, but there is no evidence of any influence after this time.

The domain-average precipitation forecast with and without prior cloud-cover ingestion was also compared against the observed precipitation averaged over all 17 AZMET stations for a 4.5-h forecast period (Fig. 8b). There is, perhaps, some evidence of a small improvement in the forecast for some hours after prior cloud ingestion, but very substantial errors remain in the magnitude of modeled precipitation and no evidence of improvement after a few hours.

Investigation was made of why the cloud fields degrade so quickly after cloud ingestion ceases. This is

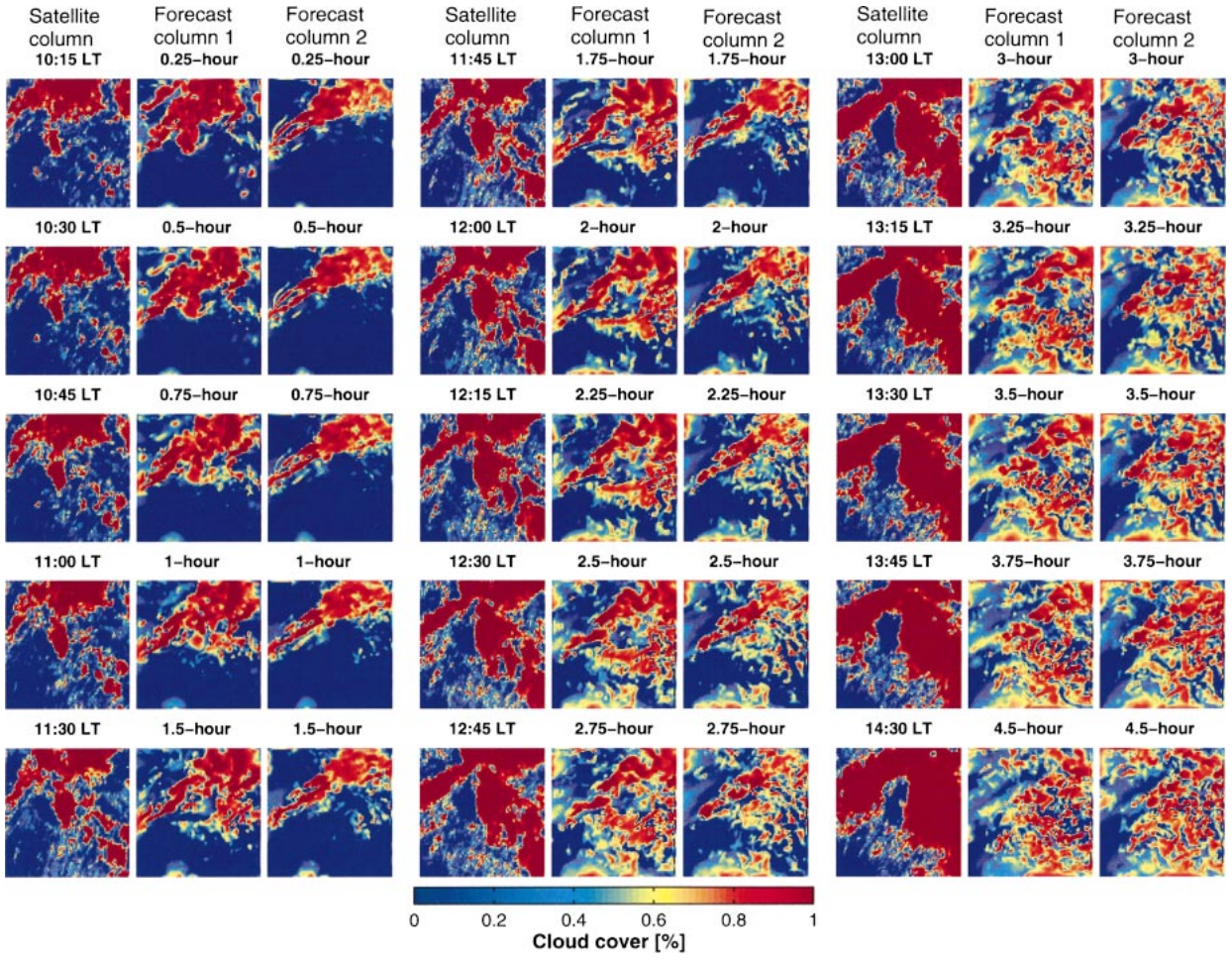

FIG. 7. Forecast fractional cloud cover with and without prior cloud assimilation compared with obs cloud fraction derived from the GOES visible images (Satellite column) at 15-min intervals during the 4.5-h forecast period. Forecast column 1 is the forecast fractional cloud cover with prior cloud assimilation, while Forecast column 2 is the forecast fractional cloud cover from the control run, both calculated over the inner model domain on 14 Jul 1999. Fractional cloud cover fields are derived from vertically integrated cloud-mass fields using an empirical relationship. LT ≡ the local time.

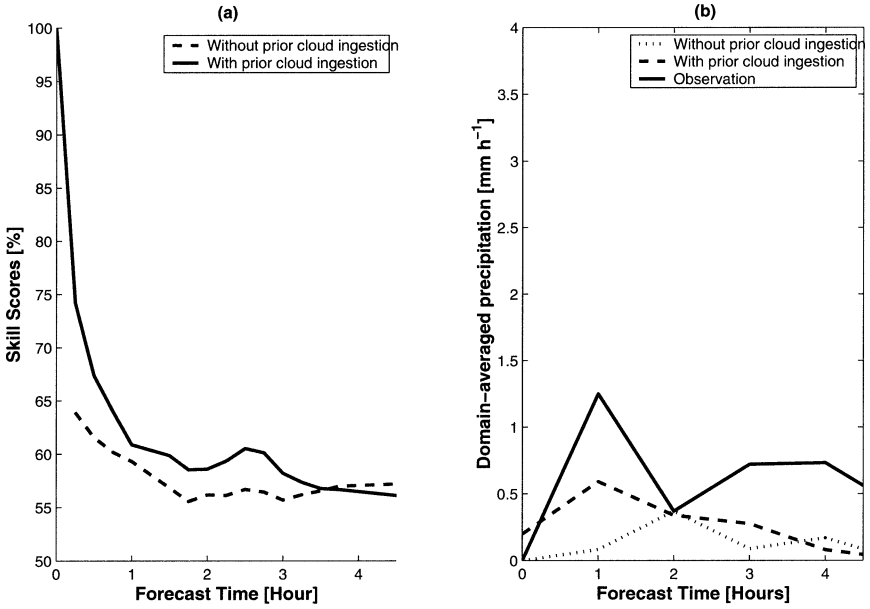

FIG. 8. Skill scores of MM5 with and without prior cloud assimilation, calculated at 15-min intervals during a 4.5-h forecast period for (a) the cloudy-only subdomains. (b) Site-average modeled with and without prior cloud assimilation and observed precipitation are compared for the forecast period of 4.5 h 14 Jul 1999. The forecast starts at 1000 and ends at 1430 LT.

likely because the vertical wind profiles and temperature and horizontal wind fields represented in MM5 are not necessarily consistent with the assimilated cloud cover at the time of assimilation. On the other hand, there is also a tendency for the model to lose the memory of inserted data due to the influence of the boundary conditions not including cloud and precipitating water. For example, studies related to the diabatic initializations of mesoscale models (Shaw et al. 2001; Shaw and Schultz 2001) report that model forecasts, which account for the presence of the hydrometeorological species in the initial conditions, had significantly improved skill in forecasting clouds and precipitation in the early hours of the forecast compared to other conventional initialization methods. Figure 9, for example, illustrates that in our study, there is inconsistency between vertical wind profiles and cloud fields at the initiation of the forecast at 1000 local time on 14 July 1999. In the study for diabatic initialization of mesoscale models by Schultz and Albers (2001), it was suggested that cloud-resolving models strongly link the convective heating rate to the local vertical wind fields and the thermodynamic energy equation. These vertical wind profiles are also coupled to the horizontal wind fields by the mass continuity equation, to define convergence or divergence. It is possible that balancing temperature fields may adjust the heating rate to give consistency between the modeled dynamical fields and the ingested cloud fields.

Figures 9a,b and 9c,d, respectively, show the cloud water/ice and the vertical wind speed across the modeled domain at model level 15 at this time. In the free-running model without cloud ingestion (Figs. 9a,c), there is clearly a strong correlation between the cloud cover and vertical wind speed at level 15. However, in the model in which cloud has previously been artificially introduced to fit the observed cloud field every 1 min for 3 h, there is little evidence that the vertical wind speed in the modeled atmosphere has responded to the introduction of cloud, and the cloud field and vertical wind speed at level 15 are largely inconsistent.

Figures 9e,f show vertical cross sections in the west–east direction of the cloud amount and vertical wind speed. These cross sections are for the west–east line shown in Figs. 9a–d. Figures 9g,h show the equivalent vertical cross sections of vertical wind speed. (Note: the lines in Figs. 9e–h indicate the model level, level 15, to which the horizontal cross sections in Figs. 9a–d correspond.) The cloud fields in the free-running model are fairly well correlated with positive vertical wind speed (upward motion), but those in the model run with prior ingestion of cloud cover are not. On the contrary, ingesting into precipitating clouds tends to make the model create downward motion in the atmosphere instantly because the model computes the liquid drag term on the vertical wind tendencies based on (ingested) precipitating hydrometeors. The liquid drag term is computed using pressure-weighted averaging. It is this inconsistency between assimilated cloud type and depth and vertical wind speed firmly tied to the convective heating rate which, we believe, causes the rapid initial degradation in forecast cloud fields (Figs. 7 and 8) in the first 15 min of the predictive run after prior cloud ingestion. After the initial rapid destruction of the assimilated cloud field in the predictive run, the model

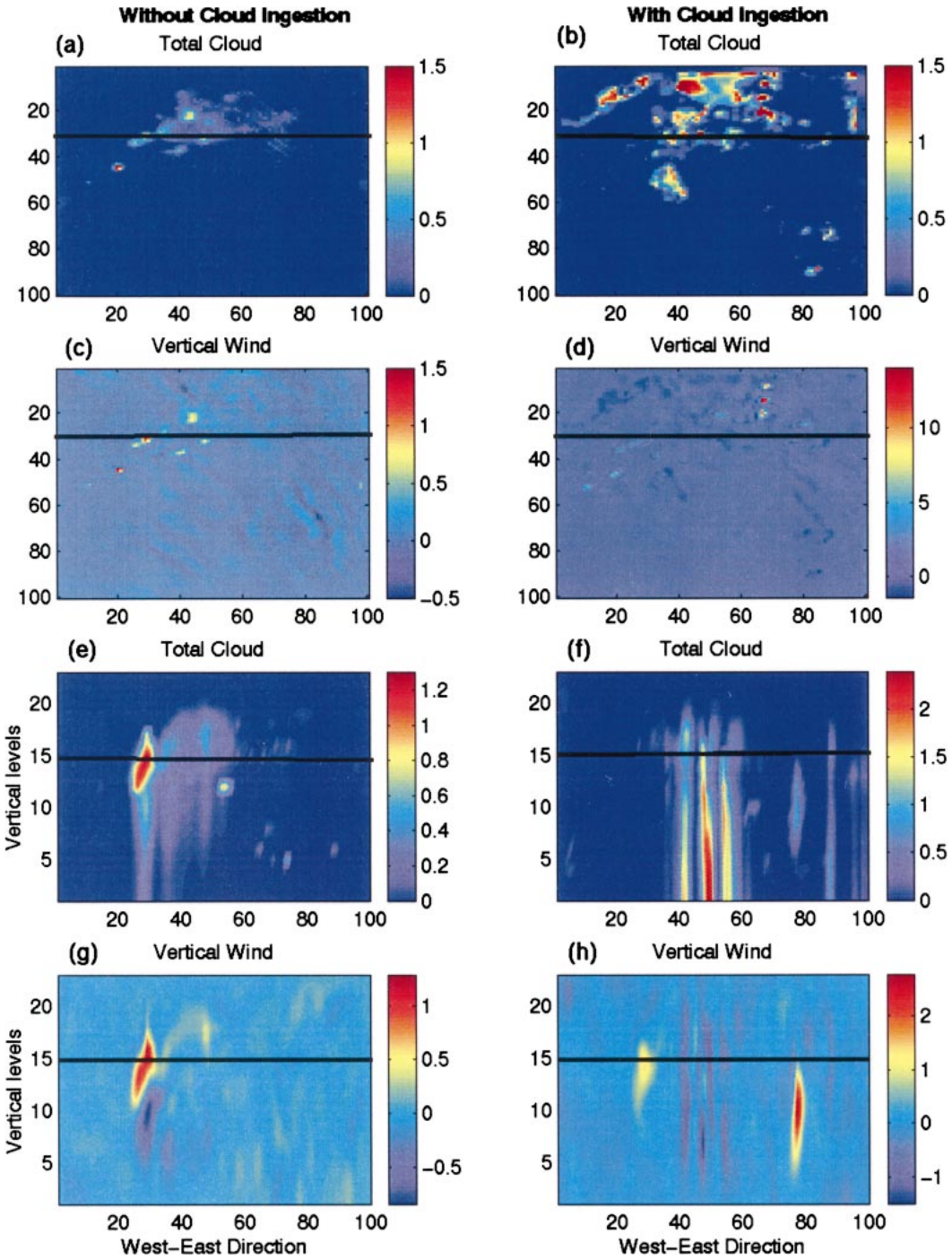

FIG. 9. The cross sections of total cloud-mixing ratio and vertical wind speed in (a)–(d) *x*–*y* and (e)–(h) *x*–*z* planes are shown for a control run of MM5 in the first column and for a run with prior cloud-cover ingestion in the second column at forecast initial time, 1000 LT. The solid thick lines show the location of the layers. The total cloud-mixing ratio is in g kg^{-1} and vertical wind speed is in m s^{-1}. The *x* axes of each subplot describe the number of grid points in the inner model domain along with longitudinal direction, while the *y* axes of each subplot from (a) to (d) describe the number of grid points in the inner model domain along with latitudinal direction.

reestablishes its own self-consistent cloud cover and wind fields. However, it does so recognizing the remnant humidity associated with the redistributed cloud water/ice introduced during the assimilation. Consequently, there is a small but general improvement in the location of clouds relative to their true (observed) location with respect to the model run without prior cloud assimilation. This improvement persists at a reasonable consistent level until chaotic processes in the model destroy the agreement between modeled and observed cloud fields.

6. Summary and conclusions

This paper describes research in which a technique was developed to assimilate finescale cloud-cover information derived from the GOES visible and infrared imager into MM5 to yield improved diagnoses of surface solar radiation and, to some extent, precipitation. By providing a realistic initialization of the cloud field in this way, the model's short-term forecasting ability is enhanced to some extent. However, this enhancement is compromised by the fact that, at the time of initiation, the cloud-cover distribution and the vertical and horizontal wind speed, and temperature fields are inconsistent, leading to rapid loss of predictive capability. To address this problem, our ongoing and future research will focus on assimilating cloud fields while simultaneously modifying the vertical wind speed profiles and the temperature and horizontal wind fields to ensure they are consistent.

The primary conclusions of the present research are as follows:

1) It is feasible to introduce a cloud-assimilation technique based on using the GOES visible and infrared data into the MM5 model without disrupting model stability, as was the case for the RAMS model (Yucel et al. 2002).
2) Explicit three-dimensional cloud fields appropriate for assimilation can be derived from remotely sensed horizontal cloud patterns, with the vertical distribution derived, in part, from the fields simulated by MM5 during the model time step immediately prior to the next assimilation and, in part, from the observed brightness temperature that allowed clouds to be distributed relative to the observed cloud-top height determined from infrared radiance of GOES.
3) Time-continuous cloud ingestion substantially increases the quality of the comparison between MM5-calculated estimates of incoming surface solar radiation and AZMET observations.
4) During time-continuous assimilation, comparison between model-calculated precipitation and AZMET observations demonstrated that the inclusion of remotely sensed cloud cover improved the timing and, to some extent, the magnitude of modeled precipitation.
5) Prior cloud-cover ingestion gives some small enhancement in the ability of MM5 to forecast cloud cover and precipitation for up to 3 h, but much forecasting skill is rapidly lost after initiation due to the initial inconsistency between the model's cloud cover and vertical wind speed fields.
6) Adjustment for model dynamics and mass fields to provide consistency with ingested cloud cover is required to improve MM5 forecast skill further.

Acknowledgments. Primary support for the research described in this paper came from NASA Grant NAG5-11044. We are grateful to Dr. Rachel T. Pinker for providing use of the UMD GEWEX/SRB model, to the AZMET program for allowing use of their data, to Efrat Morin for providing the sample radar data, to Dan Braithwaite for assistance in obtaining the required satellite datasets, and to three anonymous reviewers whose comments improved the quality of this manuscript. Thanks are also due to Corrie Thies for valuable editorial suggestions.

APPENDIX

Updating MM5 Microphysics from GOES Observations

a. Retrievals of cloud water/ice and cloud-top height from GOES observations

The UMD GEWEX/SRB model provides estimates of cloud optical depth, $\tau_{i,j}$, for the $N_i \times N_j$ (4 km $\times$ 4 km) target areas within the study area, this being determined as a function of cloudy sky radiance, $L_{i,j}$, thus,

$$\tau_{i,j} = f(L_{i,j}). \tag{A1}$$

A relationship is assumed between $m_{i,j}^{\mathrm{CL,SAT}}$, the mass (kg) of cloud water and ice in the atmosphere above the model grid square (i, j), and the satellite-derived values of cloud optical depth, with the form

$$m_{i,j}^{\mathrm{CL,SAT}} = 10^{\exp\{[\log(\tau_{i,j})-0.26]/1.71\}} ds, \tag{A2}$$

where ds is the area (m^2) of a horizontal grid square. The right-hand side of Eq. (A2) is taken from the equation derived by Stephens (1978). The corresponding cloud-top height for a given grid square is derived using the area-averaged relationship between height and temperature from MM5 as follows:

$$Z_{t_{i,j}} = f(T_{b_{i,j}}), \tag{A3}$$

where $T_{b_{i,j}}$ is the brightness temperature retrieved from GOES infrared data, which are available at 4-km spatial resolution. Each satellite target area is collocated with a 4 km $\times$ 4 km grid used in MM5 by applying a weighted interpolation between the two grid projections.

b. Representation of fractional cloud mass profiles for cloud ingestion in MM5

Prior to cloud ingestion, MM5 calculates values of air temperature, $T_{i,j,k}$, air pressure, $p_{i,j,k}$, and mixing ratios for cloud water, $r^C_{i,j,k}$, for rainwater, $r^R_{i,j,k}$, for graupel, $r^G_{i,j,k}$, for snow, $r^S_{i,j,k}$, for pristine ice, $r^P_{i,j,k}$, and for water vapor, $r^V_{i,j,k}$, respectively, at each vertical level, k, above each model grid square (i, j). The corresponding density of dry air, ρ_d (in kg m^{-3}) and vapor pressure for water vapor, e (in kPa), are calculated by the following equations:

$$\rho_d = \frac{0.622 p_{i,j,k}}{0.622 R_d T_{i,j,k} + R_d T_{i,j,k} r^V_{i,j,k}} \quad \text{and} \tag{A4}$$

$$e = \rho_d \left(\frac{R_d}{0.622} \right) r^V_{i,j,k} T_{i,j,k}, \tag{A5}$$

where R_d (=287 J kg^{-1} K^{-1}) is the dry air gas constant.

The mass of water vapor, $m^V_{i,j,k}$, and the mass of water as cloud water, $m^C_{i,j,k}$, rainwater, $m^R_{i,j,k}$, graupel, $m^G_{i,j,k}$, snow, $m^S_{i,j,k}$, and pristine ice, $m^P_{i,j,k}$, all in kg, in a parcel of the atmosphere with volume $V_{i,j,k}$ can then be calculated from their respective mixing ratios and the vapor pressure, air pressure, and temperature of the air parcel, thus,

$$m_{i,j,k} = \frac{(p_{i,j,k} - e) V_{i,j,k} r_{i,j,k}}{R_d T_{i,j,k}}. \tag{A6}$$

Depending on the satellite-retrieved brightness temperature, $T_{b_{i,j}}$ (in K) and cloud optical thickness ($\tau_{i,j}$), the total mass of cloud species produced in the atmospheric column from cloud top ($Z_{t_{i,j}}$) to cloud base ($Z_{b_{i,j}}$) above the modeled grid square is then assigned from

$$M^{\mathrm{CL,MM5}}_{i,j} = \begin{cases} \displaystyle\sum_{k=Z_b}^{Z_t} m^C_{i,j,k} + \sum_{k=Z_b}^{Z_t} m^R_{i,j,k} + \sum_{k=Z_b}^{Z_t} m^G_{i,j,k} + \sum_{k=Z_b}^{Z_t} m^S_{i,j,k} + \sum_{Z_b}^{Z_t} m^P_{i,j,k}, & T_{b_{i,j}} < 273 \text{ K} \quad \text{and} \quad \tau_{i,j} > 10 \\ \displaystyle\sum_{k=Z_b}^{Z_t} m^C_{i,j,k} + \sum_{k=Z_b}^{Z_t} m^R_{i,j,k}, & T_{b_{i,j}} > 273 \text{ K} \\ \displaystyle\sum_{k=Z_b}^{Z_t} m^P_{i,j,k}, & T_{b_{i,j}} < 250 \text{ K} \quad \text{and} \quad \tau_{i,j} \le 10, \end{cases} \tag{A7}$$

where k refers to each atmospheric level in the specified cloud layer. [Determination of cloud-base altitude (Z_b) was explained in section 4a of this paper.] If $M^{\mathrm{CL,MM5}}_{i,j}$ calculated from the previous expression, where the satellite also observes clouds, is greater than zero, the vertical cloud fraction is simply given at each vertical level by

$$f^C_{i,j,k} = \frac{m^C_{i,j,k}}{M^{\mathrm{CL,MM5}}_{i,j}}, \qquad f^R_{i,j,k} = \frac{m^R_{i,j,k}}{M^{\mathrm{CL,MM5}}_{i,j}},$$

$$f^G_{i,j,k} = \frac{m^G_{i,j,k}}{M^{\mathrm{CL,MM5}}_{i,j}}, \qquad f^S_{i,j,k} = \frac{m^S_{i,j,k}}{M^{\mathrm{CL,MM5}}_{i,j}},$$

$$f^P_{i,j,k} = \frac{m^P_{i,j,k}}{M^{\mathrm{CL,MM5}}_{i,j}}, \tag{A8}$$

where $f_{i,j,k}s$ are vertical cloud-mass profiles for cloud water, rainwater, graupel, snow, and pristine ice hydrometeors, respectively.

If $M^{\mathrm{CL,MM5}}_{i,j}$ is equal to zero (meaning that MM5 does not produce any clouds for this particular column but the satellite observes clouds), cloud water must be created at vertical levels. In this case, the total condensed cloud water calculated by the moist-adiabatic ascent from cloud base to cloud top is assumed equal to $M^{\mathrm{CL,MM5}}_{i,j}$. Because this method relies on estimating the distance between the cloud top and the cloud base by assuming a vertical distribution of cloud water between these levels, the total condensed cloud water at each vertical level, $m^C_{i,j,k}$, is calculated. The details on the calculation of condensed water are given in section 4a of this paper. These (newly created) values of cloud water can then be used to calculate the fractional mass or cloud at each vertical level in the specified cloud layer as above, that is, from

$$\left\{ f^C_{i,j,k} = \frac{m^C_{i,j,k}}{M^{\mathrm{CL,MM5}}_{i,j}}, \qquad T_{b_{i,j}} < 273 \text{ K} \quad \text{and} \quad \tau_{i,j} > 10 \right\}$$

$$\left\{ f^P_{i,j,k} = f^C_{i,j,k} = \frac{m^C_{i,j,k}}{M^{\mathrm{CL,MM5}}_{i,j}}, \qquad T_{b_{i,j}} < 250 \text{ K} \quad \text{and} \quad \tau_{i,j} \le 10 \right\}. \tag{A9}$$

In the previous expression, the calculated condensed water is assigned either to be cloud liquid water or pristine ice water in the case of cold, cirrus clouds. The fractional masses for other cloud species are set equal to zero initially, but their values quickly evolve as the model runs.

c. Updating the MM5 explicit cloud fields

Once the fractional mass or cloud at each vertical level in the specified layer of the atmospheric column has been calculated as above, the new mass of cloud water, rainwater, graupel, snow, and pristine ice in each parcel (i, j, k) of the atmosphere can be calculated from

$$(m_{i,j,k}^{C,\mathrm{MM5}})_{\mathrm{new}} = f_{k,i,j}^{C} m_{i,j}^{\mathrm{CL,SAT}}, \qquad (m_{i,j,k}^{R,\mathrm{MM5}})_{\mathrm{new}} = f_{k,i,j}^{R} m_{i,j}^{\mathrm{CL,SAT}},$$
$$(m_{i,j,k}^{G,\mathrm{MM5}})_{\mathrm{new}} = f_{k,i,j}^{G} m_{i,j}^{\mathrm{CL,SAT}}, \qquad (m_{i,j,k}^{S,\mathrm{MM5}})_{\mathrm{new}} = f_{k,i,j}^{S} m_{i,j}^{\mathrm{CL,SAT}},$$
$$(m_{i,j,k}^{P,\mathrm{MM5}})_{\mathrm{new}} = f_{k,i,j}^{P} m_{i,j}^{\mathrm{CL,SAT}}. \qquad \text{(A10)}$$

A revised mixing ratio for cloud water, rainwater, graupel, snow, and pristine ice is then recalculated from

$$r_{i,j,k} = \frac{R_d T_{i,j,k} (m_{i,j,k}^{\mathrm{MM5}})_{\mathrm{new}}}{V_{i,j,k}(p_{i,j,k} - e)}. \qquad \text{(A11)}$$

This equation is applied separately to each new mass $(m_{i,j,k})_{\mathrm{new}}$ of cloud water, rainwater, graupel, snow, and pristine ice hydrometeors to calculate their corresponding, revised mixing ratios ($r_{i,j,k}$).

If the satellite does not assign any cloud cover for a particular atmospheric column above the grid square in the modeled domain, any cloud amount previously calculated by the MM5 in that column is removed by assigning all of the components of cloud water and ice to zero. In this case, air parcel (i, j, k) of the atmosphere is represented as being all in the vapor phase. Because cloud amounts in the atmosphere modulates the atmospheric radiative heating and cooling terms, the modeled air temperature is indirectly updated after the mixing ratio of the cloud water and ice fields have been revised in accordance with satellite data.

REFERENCES

Albers, S. C., J. A. McGinley, D. L. Birkenheuer, and J. R. Smart, 1996: The Local Analysis and Prediction System (LAPS): Analyses of clouds, precipitation, and temperature. *Wea. Forecasting,* **11,** 273–287.

Chen, F., and J. Dudhia, 2001: Coupling an advanced land surface–hydrology model with the Penn State–NCAR MM5 Modeling System. Part I: Model implementation and sensitivity. *Mon. Wea. Rev.,* **129,** 569–585.

Colle, B. A., K. J. Westrick, and C. F. Mass, 1999: Evaluation of MM5 and Eta-10 precipitation forecasts over the Pacific Northwest during the cool season. *Wea. Forecasting,* **14,** 137–154.

——, C. F. Mass, and K. W. Westrick, 2000: MM5 precipitation verification over the Pacific Northwest during the 1997–99 cool seasons. *Wea. Forecasting,* **15,** 730–744.

Dudhia, J., 1989: Numerical study of convection observed during the winter monsoon experiment using a mesoscale two-dimensional model. *J. Atmos. Sci.,* **46,** 3077–3107.

——, 1993: A nonhydrostatic version of the Penn State–NCAR Mesoscale Model: Validation tests and simulation of an Atlantic cyclone and cold front. *Mon. Wea. Rev.,* **121,** 1493–1513.

Frisch, A. S., C. W. Fairall, and J. B. Snider, 1995: Measurement of stratus cloud and drizzle parameters in ASTEX with a K_α-band Doppler radar and a microwave radiometer. *J. Atmos. Sci.,* **52,** 2788–2799.

Grell, G. A., J. Dudhia, and D. R. Stauffer, 1995: A description of the fifth generation Penn State/NCAR mesoscale model (MM5). NCAR Tech. Note NCAR/TN-398+STR, 138 pp.

Hong, S.-Y., and H.-L. Pan, 1996: Nonlocal boundary layer vertical diffusion in a medium-range forecast model. *Mon. Wea. Rev.,* **124,** 2322–2339.

Kain, J. S., and J. M. Fritsch, 1992: Convective parameterization for mesoscale models: The Kain–Fritsch scheme. *The Representation of Cumulus Convection in Numerical Models, Meteor. Monogr.,* No. 46, Amer. Meteor. Soc., 165–170.

Lin, Y.-L., R. D. Farley, and H. D. Orville, 1983: Bulk parameterization of the snow field in a cloud model. *J. Climate Appl. Meteor.,* **22,** 1065–1092.

Lipton, A. E., 1993: Cloud shading retrieval and assimilation in a satellite-model coupled mesoscale analysis system. *Mon. Wea. Rev.,* **121,** 3062–3081.

——, and G. D. Modica, 1999: Assimilation of visible-band satellite data for mesoscale forecasting in cloudy conditions. *Mon. Wea. Rev.,* **127,** 265–278.

Liu, Y., D.-L. Zhang, and M. K. Yau, 1997: A multiscale numerical study of hurricane Andrew (1992). Part I: Explicit simulation and verification. *Mon. Wea. Rev.,* **125,** 3073–3093.

Orville, H. D., and F. J. Kopp, 1977: Numerical simulation of the history of a hailstorm. *J. Atmos. Sci.,* **34,** 1596–1618.

Pinker, R. T., and I. Laszlo, 1992: Modeling surface solar irradiance for satellite applications on a global scale. *J. Appl. Meteor.,* **31,** 194–212.

Ruggiero, F. H., G. D. Modica, and A. E. Lipton, 2000: Assimilation of satellite imager data and surface observations to improve analysis of circulations forced by cloud shading contrasts. *Mon. Wea. Rev.,* **128,** 434–448.

Schultz, P., and S. Albers, 2001: The use of three-dimensional analyses of cloud attributes for diabatic initialization of mesoscale models. Preprints, *14th Conf. on Numerical Weather Prediction,* Fort Lauderdale, FL, Amer. Meteor. Soc., J122–J124.

Shaw, B. L., and P. Schultz, 2001: Explicit initialization of clouds and precipitation and implications for microphysical parameterizations. Preprints, *11th PSU/NCAR Mesoscale Users' Workshop,* Boulder, CO, NCAR, 74–77.

——, J. A. McGinley, and P. Schultz, 2001: Explicit initialization of clouds and precipitation in mesoscale forecast models. Preprints, *14th Conf. on Numerical Weather Prediction,* Fort Lauderdale, FL, Amer. Meteor. Soc., J87–J91.

Smith, W. P., and R. L. Gall, 1989: Tropical squall lines of the Arizona monsoon. *Mon. Wea. Rev.,* **117,** 1553–1569.

Smolarkiewicz, P., and G. A. Grell, 1992: A class of monotone interpolation schemes. *J. Comput. Phys.,* **101,** 431–440.

Stephens, G. L., 1978: Radiation profiles in extended water clouds. II: Parameterization schemes. *J. Atmos. Sci.,* **35,** 2123–2132.

Tao, W.-K., and J. Simpson, 1993: The Goddard cumulus ensemble model. Part I: Model description. *Terr. Atmos. Oceanic Sci.,* **4,** 35–72.

Watson, A. I., R. E. Lopez, and R. L. Holle, 1994: Diurnal cloud-to-ground lightning patterns in Arizona during the southwest monsoon. *Mon. Wea. Rev.,* **122,** 1716–1725.

Whitlock, C. H., and Coauthors, 1995: First global WCRP shortwave surface radiation budget dataset. *Bull. Amer. Meteor. Soc.,* **76,** 905–922.

Yucel, I., W. J. Shuttleworth, R. T. Pinker, L. Lu, and S. Sorooshian, 2002: Impact of ingesting satellite-derived cloud cover into the Regional Atmospheric Modeling System. *Mon. Wea. Rev.,* **130,** 610–628.